Use of Adaptive Diffusion Filters to Estimate In-Vivo Conductivity Images from B1+ Maps

Eric Michel[1], Daniel Hernandez[1], Min Hyoung Cho[1], and Soo Yeol Lee[1]
[1]*Dept. of Biomedical Engineering, Kyung Hee University, Yongin-Si, Gyeonggi-Do, Korea*

Target audience: This work is relevant to those interested in electric property tomography.

Introduction: Non-invasive Electric Properties Tomography (EPT) is believed to play a great role in local SAR estimation, malicious tissue identification and electric cancer therapy. Recent EPT methods are based on variations of the Maxwell's equations in which the electric property maps are computed from the transmit RF field (B_1^+) maps assuming homogeneous media distribution [1]. The relation between B_1^+ and σ is governed by the Helmholtz equation shown in Eq. (1). Numerical solutions to this equation in previous studies [2-3] had shown favorable results in noise-free cases. They used modified versions of the discrete Laplacian operator (∇^2) to deal with noisy B_1^+ maps, but this reduces the precision of the Laplacian estimation degrading the accuracy of the electrical property maps. Instead, we propose to use a non-linear anisotropic diffusion filter (ADF) to denoise the B_1^+ maps prior to the Laplacian computation.

$$\sigma = \frac{1}{\mu\omega}\mathrm{Im}\left(\frac{\nabla^2(B_1^+)}{B_1^+}\right) \quad (1)$$

Methods: We used the iterative 3D ADF shown in Eq. (2) to obtain a denoised version of the B_1^+ maps ($\tilde{B}_1^+$) where Δt is the factor of diffusion speed, k is the noise identification factor for a given pixel, d is the direction of the gradient ∇_d [4]. After denoising, we used the conventional central difference equations along the x-, y- and z-directions to compute the second order derivatives, and then added them to get the Laplacian. An example for the x-directional derivative is shown in Eq. (3) where h_x represents the x-directional pixel size. After Laplacian computations, we used Eq. (1) to get the conductivity maps. We also implemented the numerical solutions proposed by van Lier [2] and Bulumulla [3] for performance comparison. Van Lier's method is based on the noise-robust Laplacian 3-D kernel operators (the size of 5x3x3 for the lateral direction and 7x3x3 for the in-plane directions) while Bulumulla's method is based on skip factors in computing the second order derivatives. We performed FDTD simulations on a high-pass birdcage coil with 16 rungs tuned at 123.5 MHz using SEMCAD X (SPEAG, Switzerland). We set an isotropic grid for a FOV of 300x300x300mm with a total matrix size of 128x128x32. We computed B_1^+ field inside a double cylindrical phantom (radius=47mm, height=158mm) that had electric conductivities of 0.2 and 1.8 S/m (L and H in Fig. 1a, respectively) and a relative permittivity of 76.7. We also computed B_1^+ field in the synthetic human head model with the same pixel size. We performed in-vivo imaging experiments at 2.9T MRI using the double angle method (DAM) to obtain B_1^+ magnitude and phase maps of a volunteer's head placed in a high-pass birdcage coil that had the same shape as the one in the FDTD simulation (scan parameters: FOV=300mm, THK=10mm, matrix size=128x128, TE=20ms, TR=5s, FA=60°/120°).

$$\tilde{B}_1^+[n+1] = \tilde{B}_1^+[n] + \Delta t \sum_{d\in(x,y,z)} k \cdot \nabla_d \tilde{B}_1^+[n] \quad (2)$$

$$D_x(x,y,z) = \frac{-2\tilde{B}_1^+(x,y,z) + \tilde{B}_1^+(x+1,y,z) + \tilde{B}_1^+(x-1,y,z)}{h_x^2} \quad (3)$$

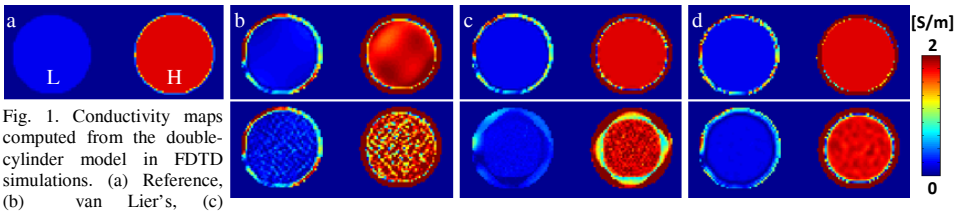

Fig. 1. Conductivity maps computed from the double-cylinder model in FDTD simulations. (a) Reference, (b) van Lier's, (c) Bulumulla's and (d) the proposed method.

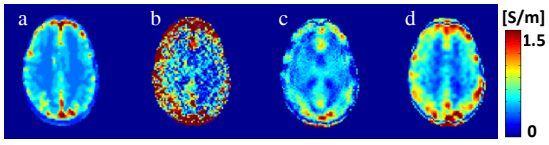

Fig. 2. Simulated conductivity maps of a human head model. (a) Reference, (b) van Lier's, (c) Bulumulla's and (d) the proposed method.

Results: From the FDTD simulation data, we extracted the magnitude and phase maps of the B_1^+ field. We computed the reference conductivity maps by $\sigma = J/E$ as shown in Fig. 1a. Figures 1b-1d show the conductivity maps computed by the three methods. The top images have been computed from the noise-free B_1^+ maps while the bottom images from the B_1^+ maps after adding white Gaussian noise (SD=0.005 when peak B_1^+ is normalized to one). Figure 2 shows the conductivity maps of a human head model (Fig. 2b-2d) along with the reference map (Fig. 2a) computed from the noisy B_1^+ maps (SD=0.005). As can be seen from the figures, all the three methods give good estimation from the noise-free B_1^+ maps, but the proposed method works better in noisy cases. Figure 3 shows the conductivity maps (Fig. 3b-3d) in the volunteer's head along with the corresponding T_1-weighted image (Fig. 3a). We observed that 3 iterations were enough for denoising the simulated B_1^+ maps, while 8 iterations were necessary for denoising the measured B_1^+ maps. The mean conductivity values along with the standard deviations at different homogeneous regions of 200 pixels are shown in Table 1.

Discussion and conclusions: The adaptive diffusion filter effectively removed the noise from the B_1^+ maps while preserving important detail structures allowing us to use a more conventional central difference Laplacian operator that worked on three consecutive neighboring pixels. This enabled us to obtain higher resolution conductivity maps for in-vivo EPT applications. From both simulation and experiments, we observed higher similarity between the reference conductivity maps and the conductivity maps computed by the proposed method. High accuracy Laplacian computation with less noise effects seems to significantly improve EPT results.

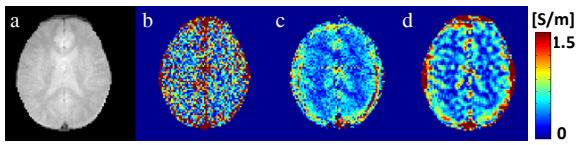

Fig. 3. In-vivo images. (a) T1-weighted image. Conductivity maps using (b) van Lier's, (c) Bulumulla's and (d) the proposed method.

Material	Reference	Estimation Method		
		Van Lier	Bulumulla	Proposed
Cylinder L	0.2	0.16[0.18]	0.23[0.09]	0.21[0.03]
Cylinder H	1.8	1.69[0.29]	1.89[0.15]	1.83[0.09]
Gray matter	0.58	0.72[0.34]	0.64[0.19]	0.61[0.12]
White matter	0.34	0.51[0.26]	0.41[0.17]	0.33[0.10]
CSF	2.14	2.92[0.38]	2.86[0.25]	2.27[0.16]

Table 1. Mean conductivity comparison between the three methods shown in Fig. 1 (bottom) and Fig. 2. All the quantities are expressed in S/m. [*] standard deviations at each ROI.

References: [1] Katscher *et al*., IEEE Trans Med Imag **28**:1365-1374, 2009 [2] Van Lier, et al. Magn Reson Med **67**:552-561, 2012 [3] Bulumulla, et al. Concepts Magn Reson **41B**:13-21, 2012 [4] Michel, et al. Biomed Eng Online **10**:47, 2011.